BULLETIN OF THE EARTHQUAKE
RESEARCH INSTITUTE
Vol. 37 (1959), pp. 89-121

6. *Observations of Seismic Waves from Four Explosions near the Kamaisi Mine.*

By The Research Group for Explosion Seismology.

(Read Dec. 23, 1958.—Received Dec. 27, 1958.)

1. Data of observations.

As stated in other papers,[1] the boundary between a layer with *P*-wave velocity 5.75～5.85 km/sec and one with 6.10～6.20 km/sec on the west side of the Kamaisi mine was calculated to have a probable dip 6°～11° rising eastward. In order to determine more precisely its position and the form near its shallowest point, we set off four explosions as in Table 1.

Table 1.

Shot Point	Latitude	Longitude	Height	Shot time	Amount of charge
A Dôsen	39°14′24.8″	141°46′ 0.6″	380m	1954, May 1, 1h35m00.28 s	0.1ton.
B Sin'yama	17 36.7	41 31.6	360	3 35 00.513	1.0
C Daidô	14 32.5	41 23.9	530	3, 1 35 00.170	0.1
D Takinosawa	15 54.1	54 55.2	2	3 35 00.513	1.0

All four explosions were observed at stations and by observers common to all of them. Positions of shot points and observation stations are as shown in Fig. 1, and tabulated in Table 2, with additional data of instruments.

Examples of seismograms are shown in Fig. 2～17.

The positions were determined by the method of aerial photography and the plane table survey. The maximum error of the horizontal distance is about 10 m and that of the height is 2 m. The accuracy of the relative time is within the limit of 1/100 sec.

Results of measurements are shown in Table 3.

Travel times for each shot are shown respectively in Fig. 18, Fig. 19, Fig. 20, and Fig. 21.

1) Research Group for Explosion Seismology, *Pub. Bureau Central Séismologique International. Série A. Travaux Scientifiques*, **19** (1954) 229-242; T. Matuzawa, *Bull. Earthq. Res. Inst.*, **37** (1959).

Table 2.

Observation point		Location			Electro-magnetic Seismometer	Observers
		Latitude	Longitude	Height		
1. SIN'YAMA	a	39°17′32.9″	141°41′35.7″	350 m	3 c/s Vertical-4	Omote Kobayashi, Saito
	b	18.5	42 9.5	350		
	c	3.7	41.6	350		
	d	16 54.5	43 3.7	302		
2. ÔHASI	a	16 28.0	43 24.0	230	3 c/s Vertical-1 2 c/s Hor.-2	Mikumo, Otsuka, Tanaka
	b			255		
3. ÔMATU	a	15 15.9	44 21.8	190	3 c/s Vertical-5	Mine Ishigaki Shima
	b	8.4	44.9	180		
	c	13.8	44.6	175		
4. DÔSEN	a	14 49.0	46 10.8	102	3 c/s Vertical-3	Suzuki, Den, Haseba
	b	42.5	6.5	120		
	c	47.3	19.5	118		
	d	47.7	37.1	122		
	e			102		
5. MATUKURA		15 13.0	48 3.7	60	3 c/s Vertical-1	Shima, Shibano
6. NODA	a	15 23.6	49 17.4	70	3 c/s Vertical-3	Asano, Yanagisawa
	b	22.9	17.4	45		
7. KOSANO	a	15 45.5	50 22.4	35	2 c/s Hor.-3	Okano, Morimoto
	b	46.2	29.3	34		
8. NAKATUMA		16 16.7	51 33.4	26	3 c/s V-2, 3c/s H-1	Matumoto, Karakama
9. TAKINOSAWA	a	16 0.8	54 49.2	2	3 c/s Vertical-3	Murauchi, Honda, Asanuma
	b			2		
	c			2		
	d			2		
	e			4		

(to be continued)

(continued)

10. KAMAISI-KÔ	a	15 55.2	53 34.2	−4	Morishita
	b			−4	
11. URESI		15 35.7	53 35.2	7	3 c/s V–1, 10 c/s H–1	Kasahara, Sato
12. TÔNI		12 23.9	53 36.4	5	3 c/s V–1, 3 c/s H–1	Noritomi, Takagi
13. OKIRAI		6 51.8	49 5.1	19	3 c/s Vertical–4	Tazime, Akamatu, Oguchi, Ueda
14. HIKOROITI	a	7 24.3	40 41.4	82	3 c/s Vertical–3	Utsu, Usami
	b	26.9	37.4	82		
	c	26.9	37.4	82		
15. DAIDÔ	a	14 35.1	41 42.6	520	3 c/s Vertical–1	Furuya
	b	29.5	23.6	520	30 c/s Vertical–3	Ogawa
	c	23.9	10.5	520		Suyehiro
	d	23.6	10.0	520		
16. ASIGASE	a	15 35.2	39 45.9	512	P–11	Yamazaki, Kobayashi, Daikubara
	b			508		
	c			505		
	d			504		
	e			503		
	f			501		
	g			500		
	h			500		
	i			501		
	j			501		
	k			502		
	l			502		
17. TÔNO		18 9.6	32 21.0	303	3 c/s V–1, 3 c/s H–1	Hori, Tsujiura

Different pick-up positions belonging to one observation point are made out by symbols a, b, c, ...

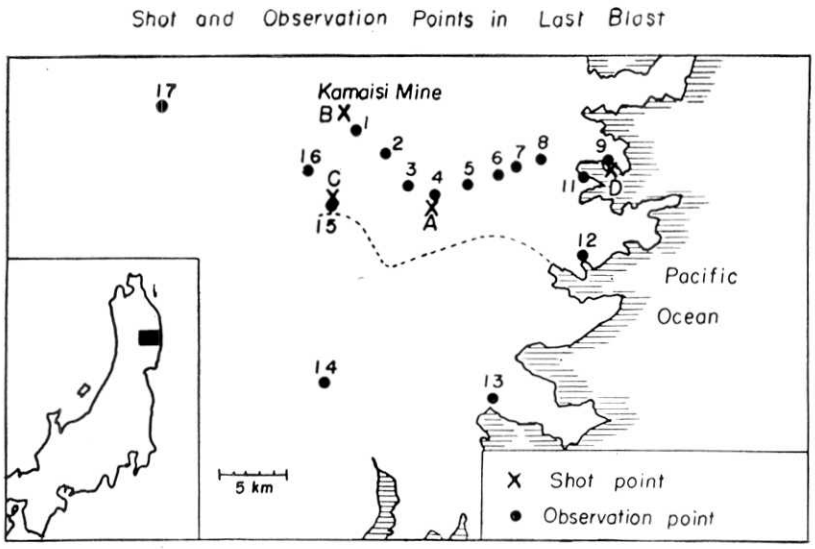

Fig. 1.

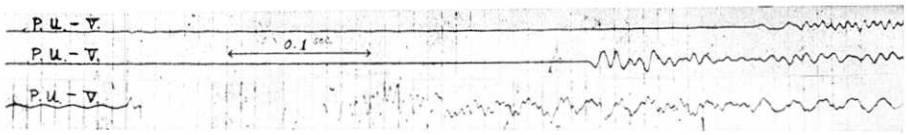

Fig. 2. Seismogram at Sin'yama for shot B.

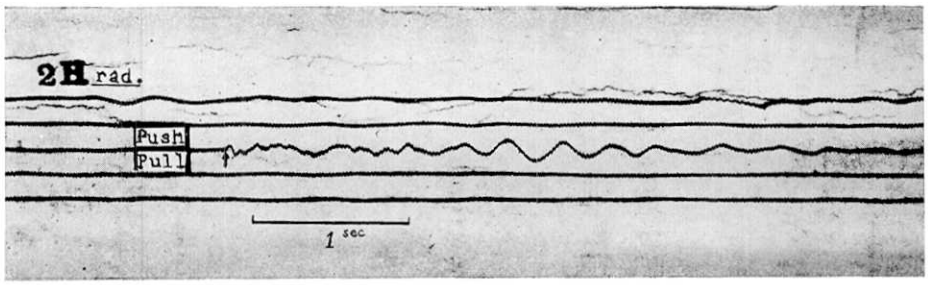

Fig. 3 (1). Seismogram at Ôhasi for shot A.

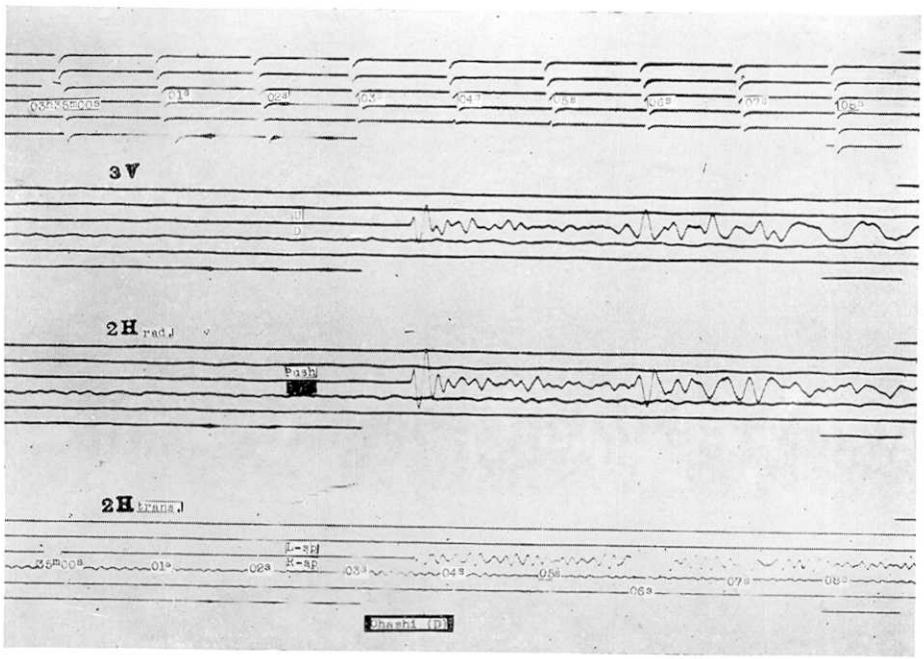

Fig. 3 (2). Seismogram at Ôhasi for shot D.

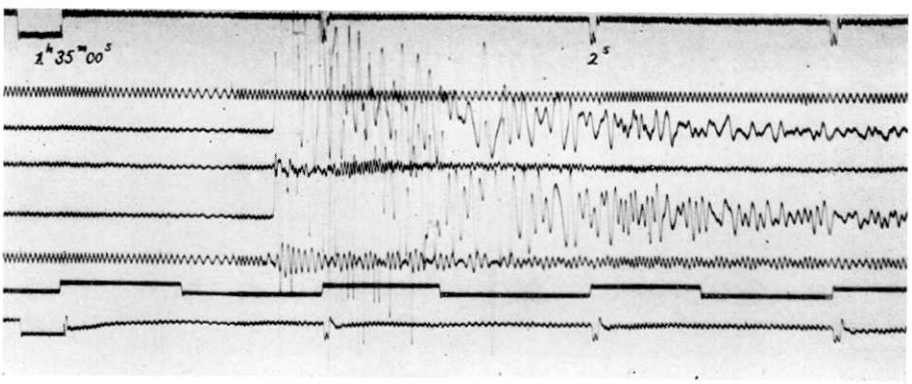

Fig. 4 (1). Seismogram at Ômatu for shot A.

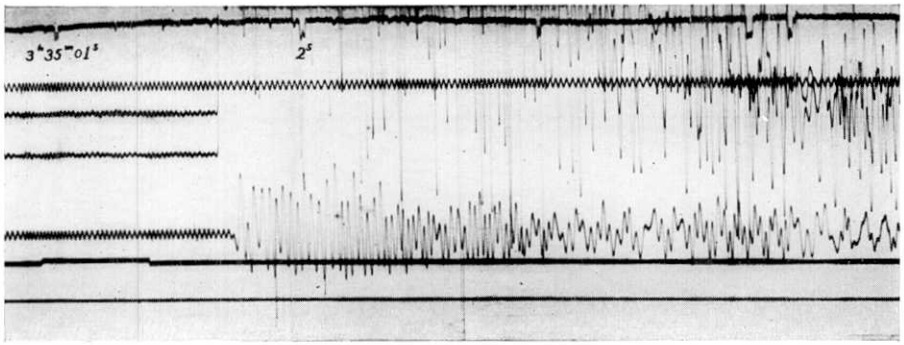

Fig. 4 (2). Seismogram at Ômatu for shot B.

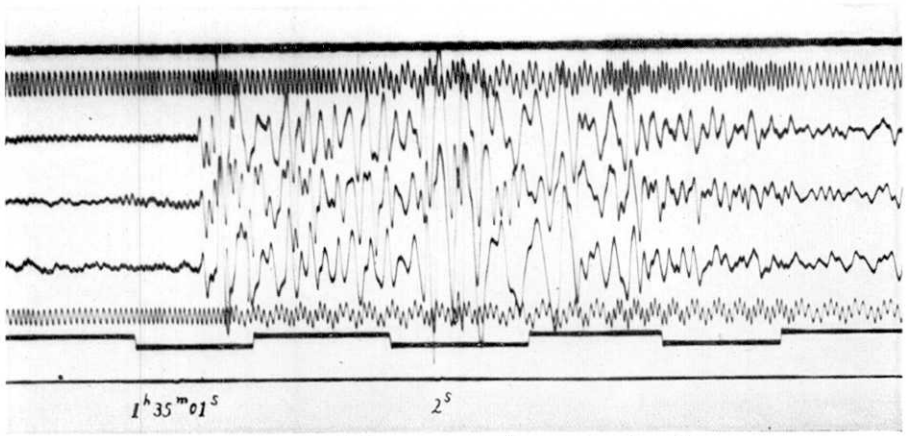

Fig. 4 (3). Seismogram at Ômatu for shot C.

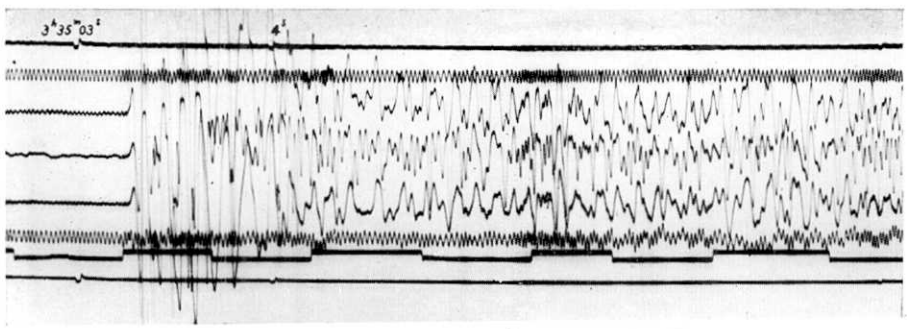

Fig. 4 (4). Seismogram at Ômatu for shot D.

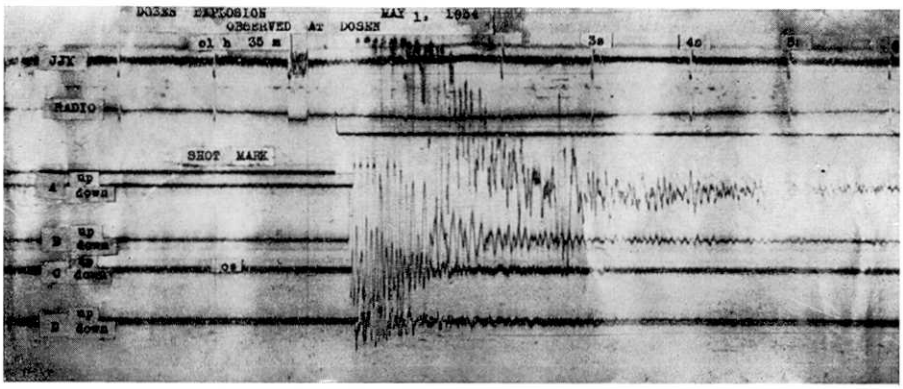

Fig. 5 (1). Seismogram at Dôsen for shot A.

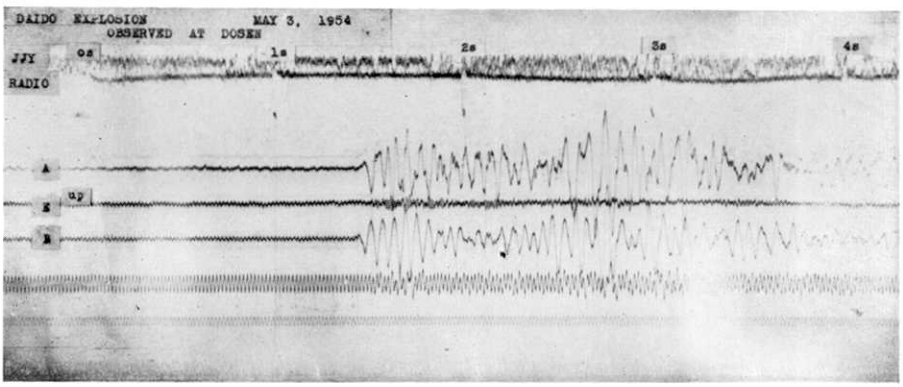

Fig. 5 (2). Seismogram at Dôsen for shot C.

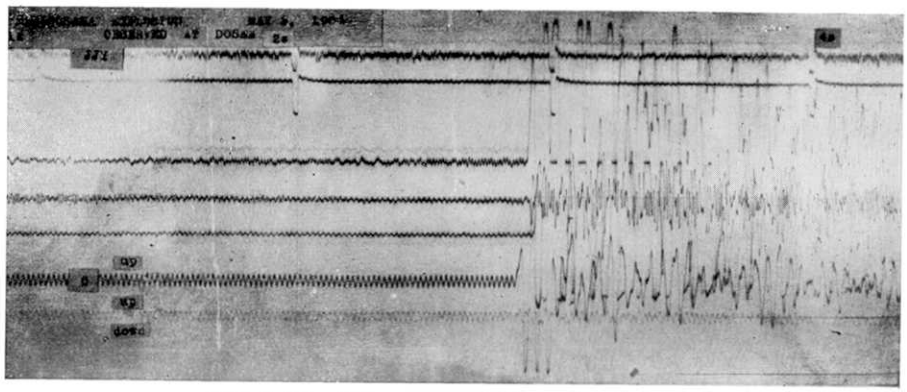

Fig. 5 (3). Seismogram at Dôsen for shot D.

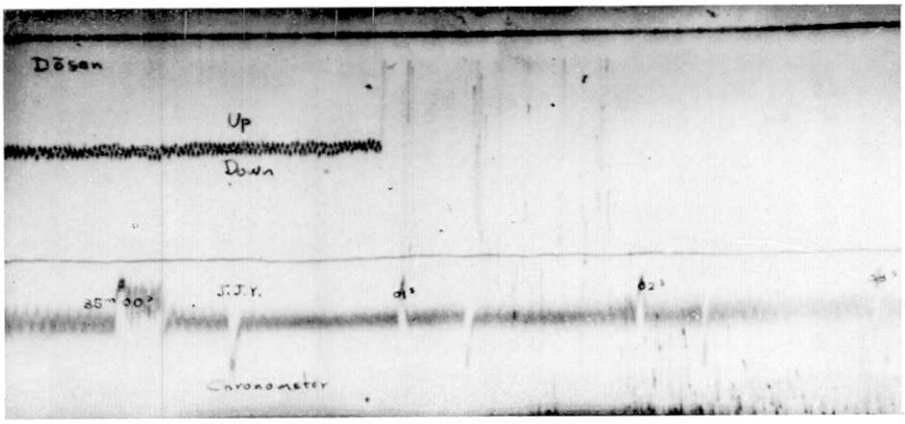

Fig. 6. Seismogram at Matukura for shot A.

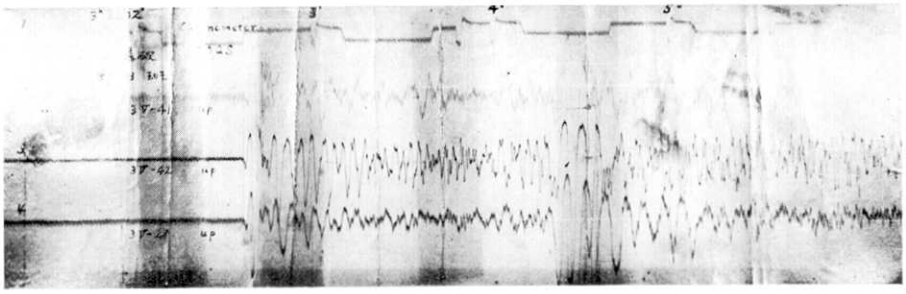

Fig. 7 (1). Seismogram at Noda for shot B.

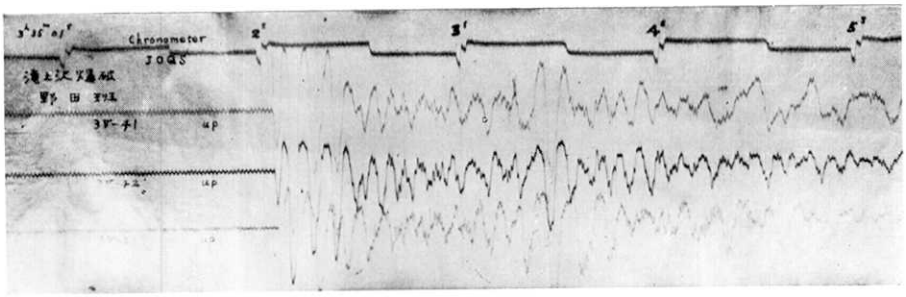

Fig. 7 (2). Seismogram at Noda for shot D.

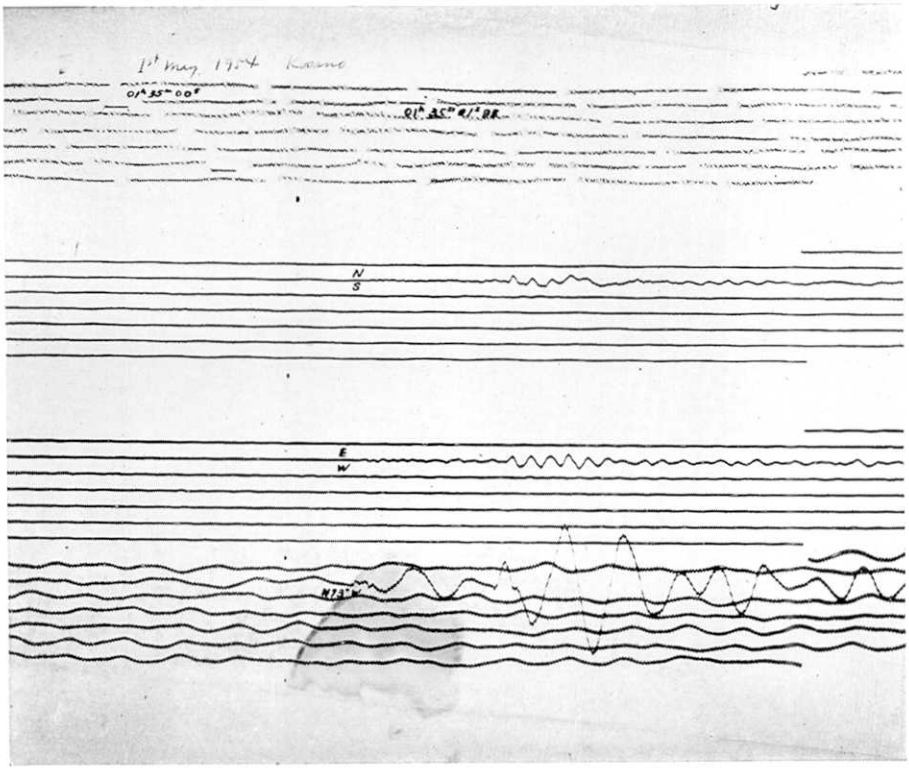

Fig. 8 (1). Seismogram at Kosano for shot A.

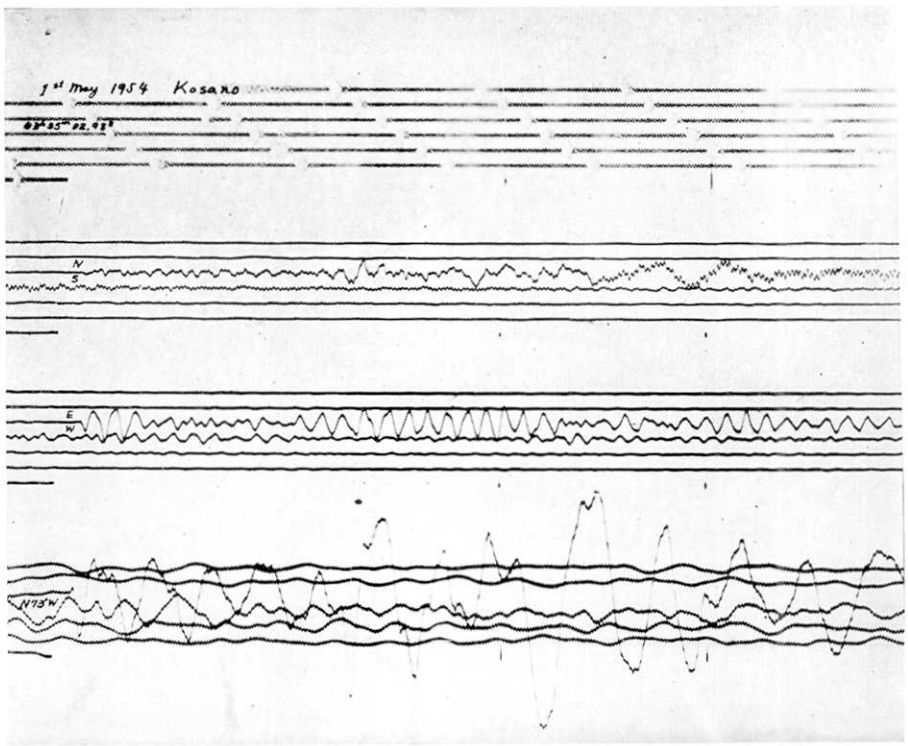

Fig. 8 (2). Seismogram at Kosano for shot B.

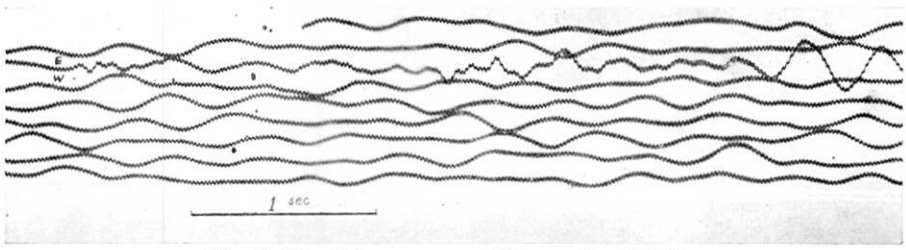

Fig. 8 (3). Seismogram at Kosano for shot C.

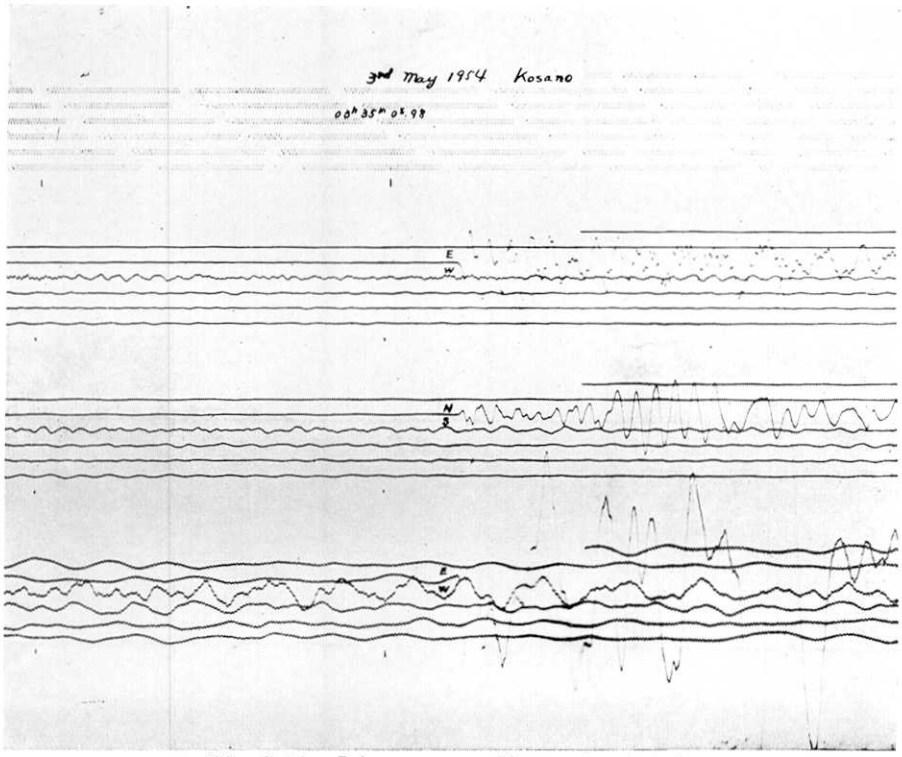

Fig. 8 (4). Seismogram at Kosano for shot D.

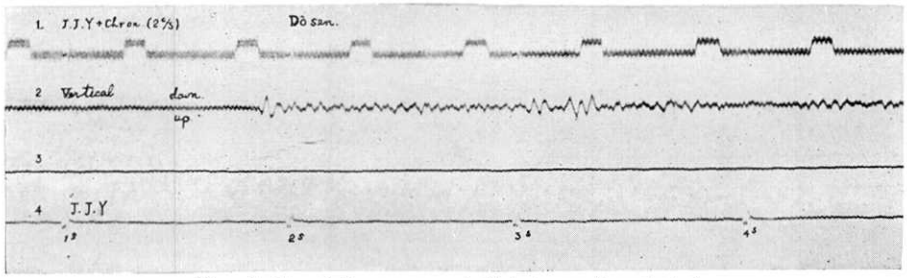

Fig. 9 (1). Seismogram at Nakatuma for shot A.

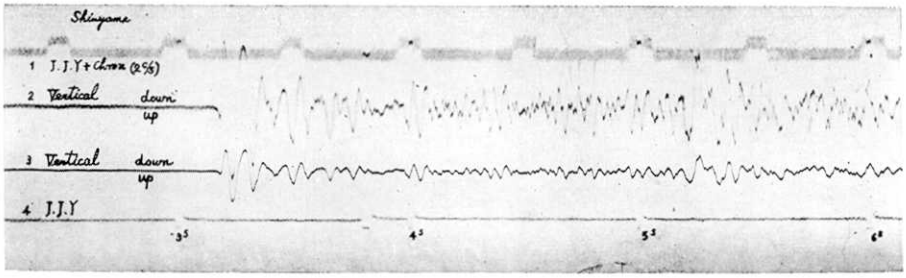

Fig. 9 (2). Seismogram at Nakatuma for shot B.

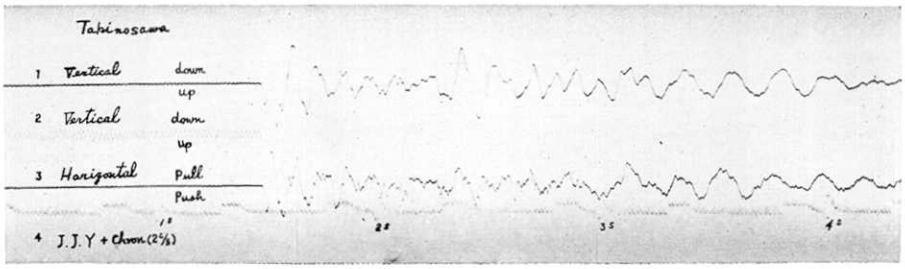

Fig. 9 (3). Seismogram at Nakatuma for shot D.

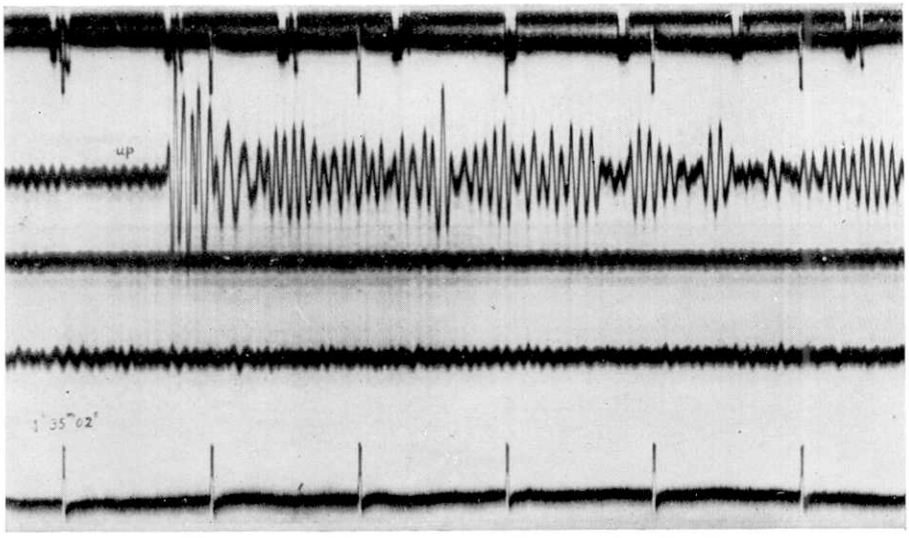

Fig. 10 (1). Seismogram at Takinosawa for shot A.

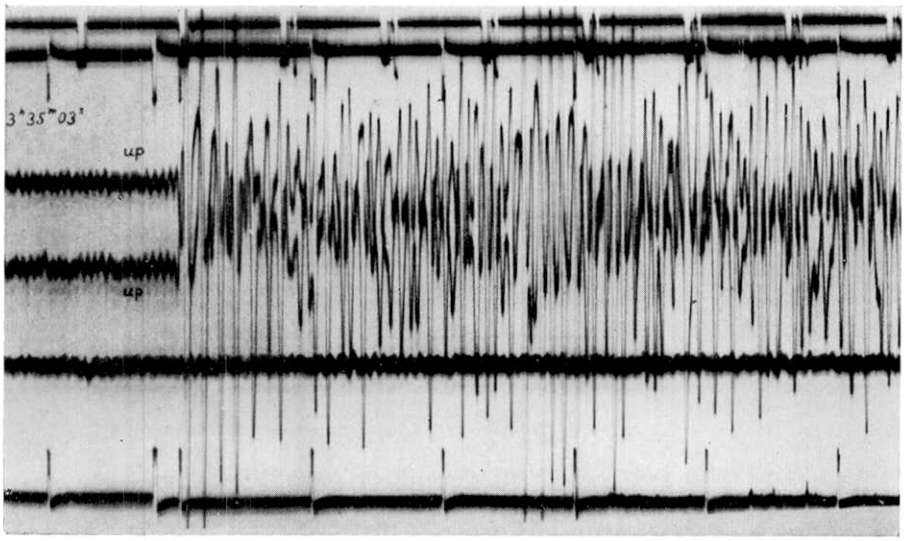

Fig. 10 (2). Seismogram at Takinosawa for shot B.

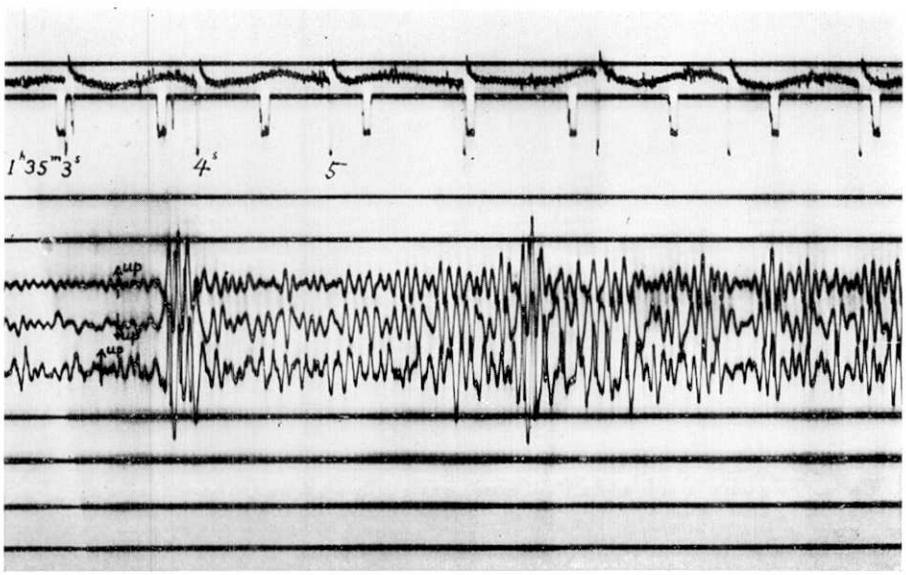

Fig. 10 (3). Seismogram at Takinosawa for shot C.

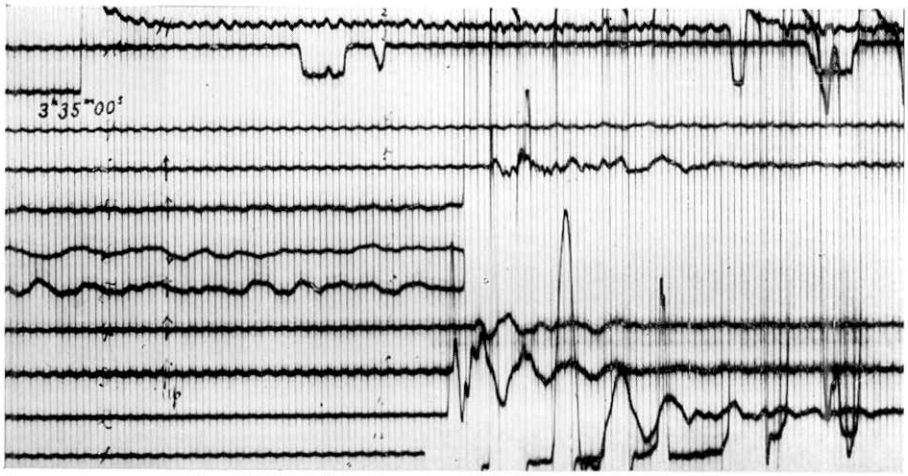

Fig. 10 (4). Seismogram at Takinosawa for shot D.

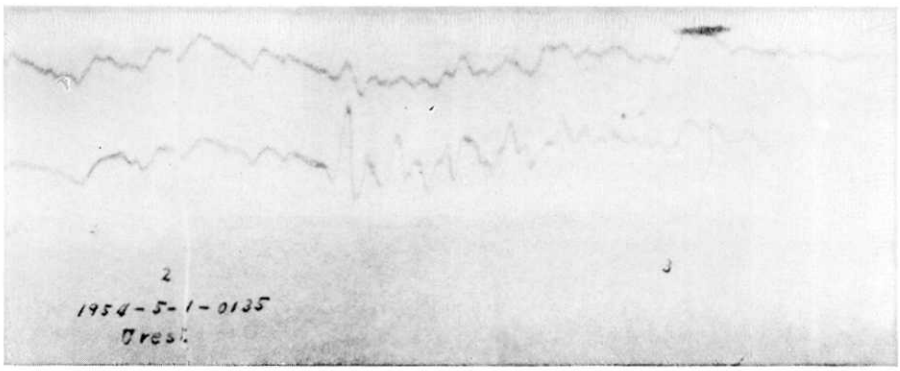

Fig. 11 (1). Seismogram at Uresi for shot A.

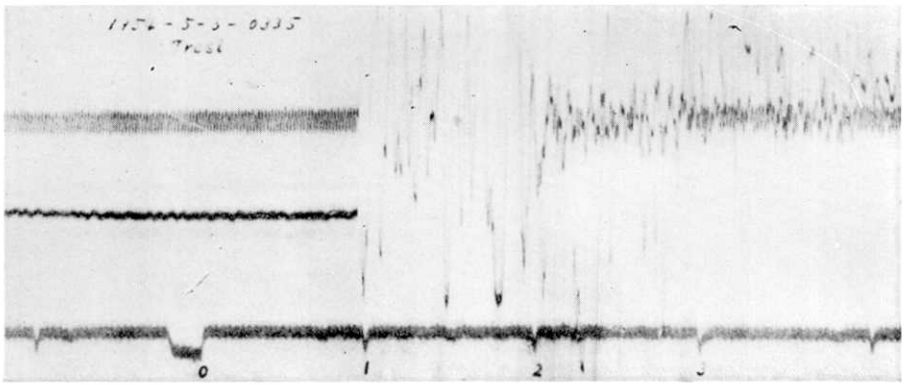

Fig. 11 (2). Seismogram at Uresi for shot D.

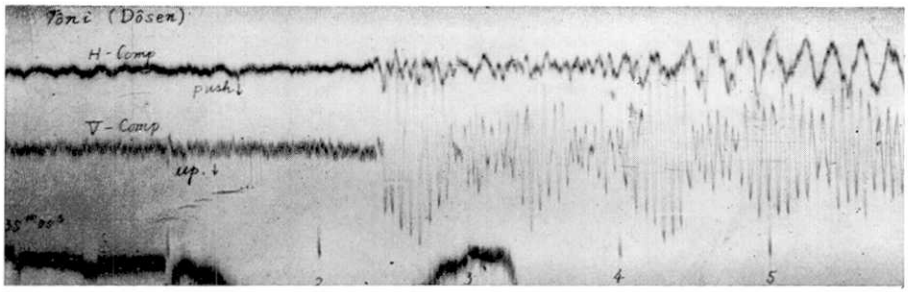

Fig. 12 (1). Seismogram at Tôni for shot A.

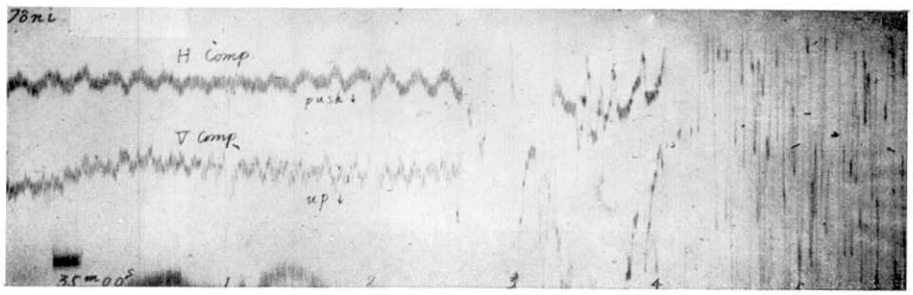

Fig. 12 (2). Seismogram at Tôni for shot B.

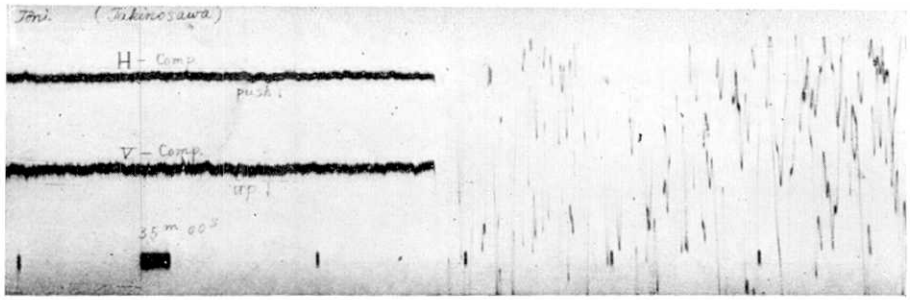

Fig. 12 (3). Seismogram at Tôni for shot D.

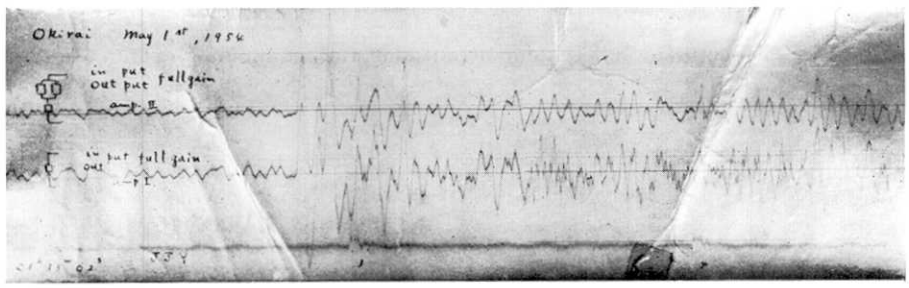

Fig. 13 (1). Seismogram at Okirai for shot A.

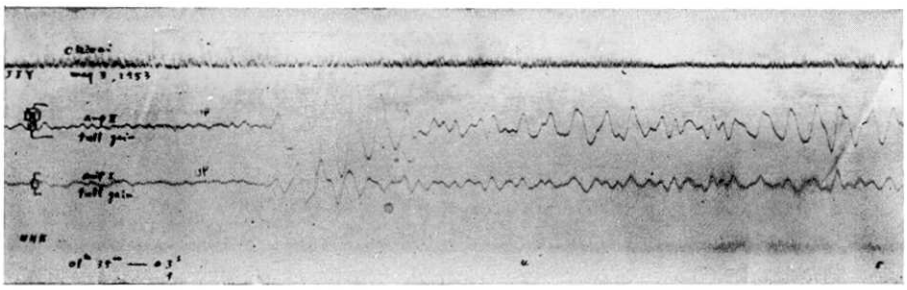

Fig. 13 (2). Seismogram at Okirai for shot C.

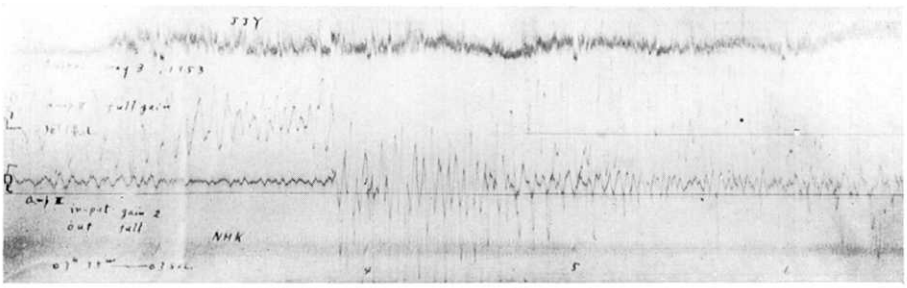

Fig. 13 (3). Seismogram at Okirai for shot D.

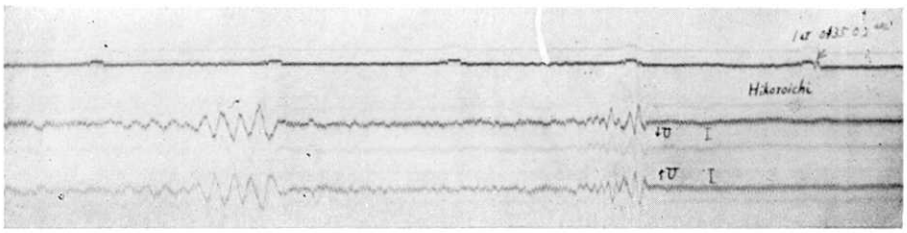

Fig. 14 (1). Seismogram at Hikoroiti for shot A.

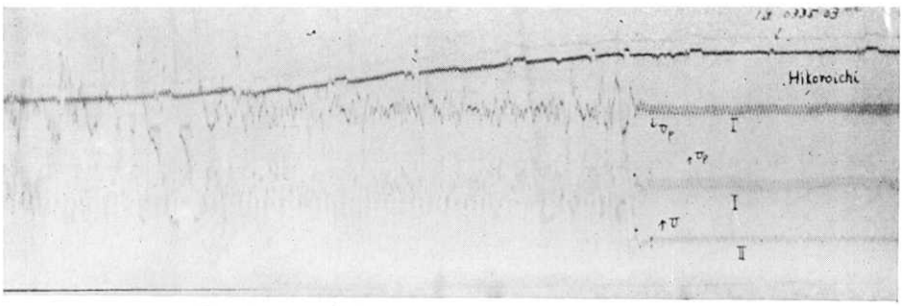

Fig. 14 (2). Seismogram at Hikoroiti for shot B.

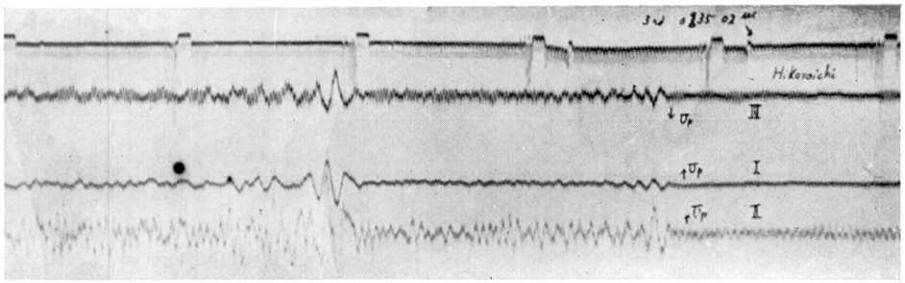

Fig. 14 (3). Seismogram at Hikoroiti for shot C.

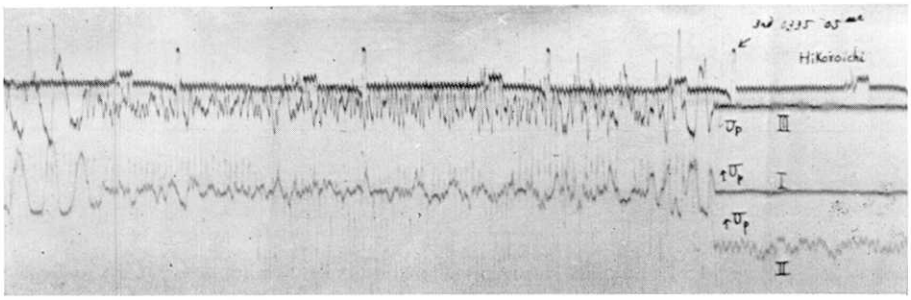

Fig. 14 (4). Seismogram at Hikoroiti for shot D.

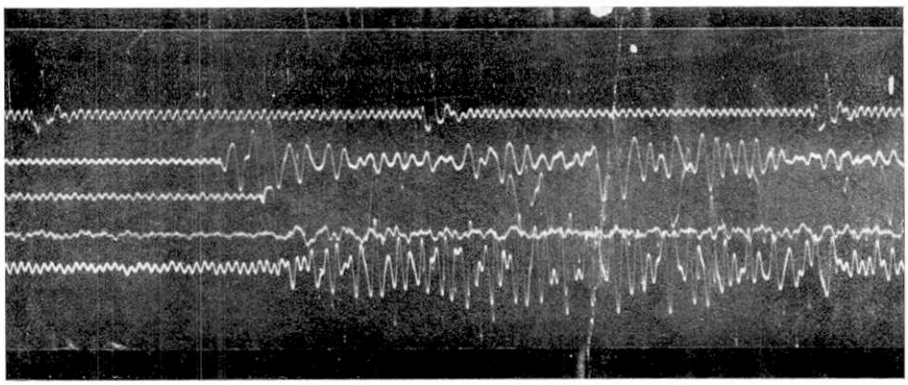

Fig. 15 (1). Seismogram at Daidô for shot A.

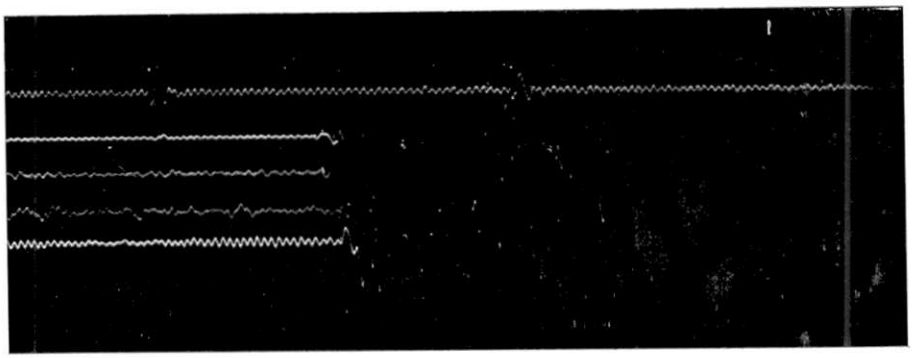

Fig. 15 (2). Seismogram at Daidô for shot B.

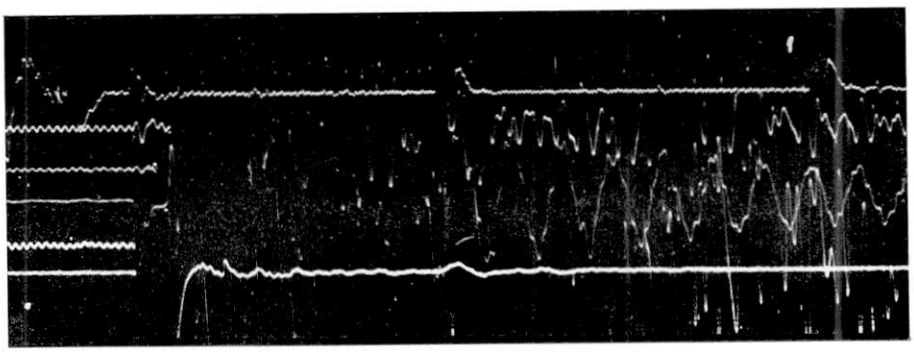

Fig. 15 (3). Seismogram at Daidô for shot C.

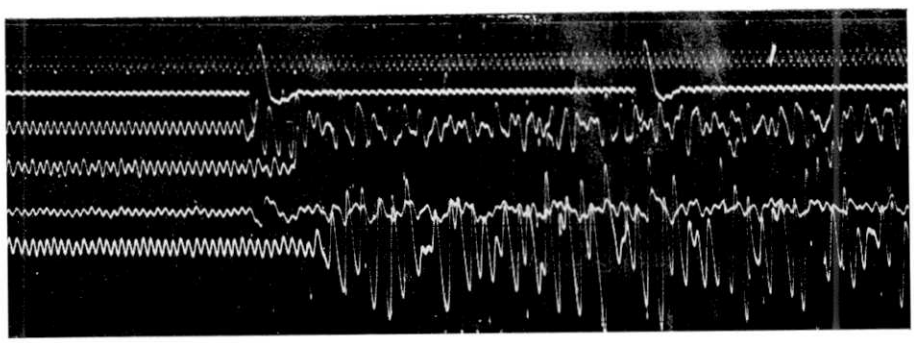

Fig. 15 (4). Seismogram at Daidô for shot D.

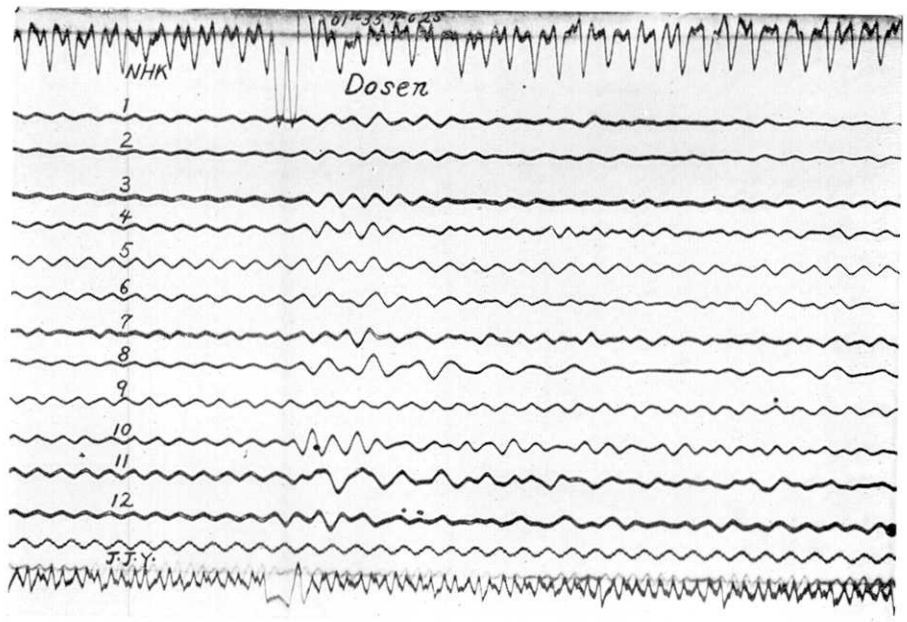

Fig. 16 (1). Seismogram at Asigase for shot A.

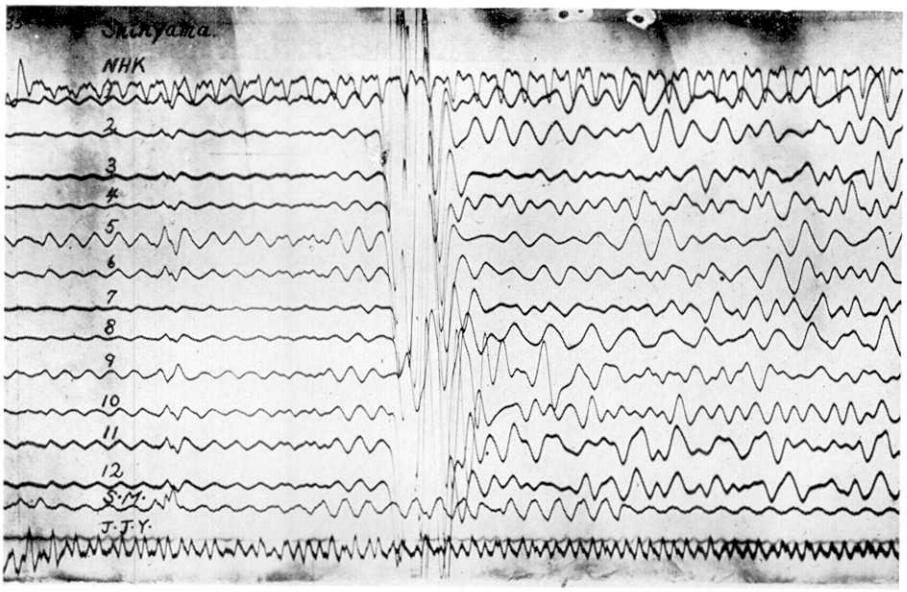

Fig. 16 (2). Seismogram at Asigase for shot B.

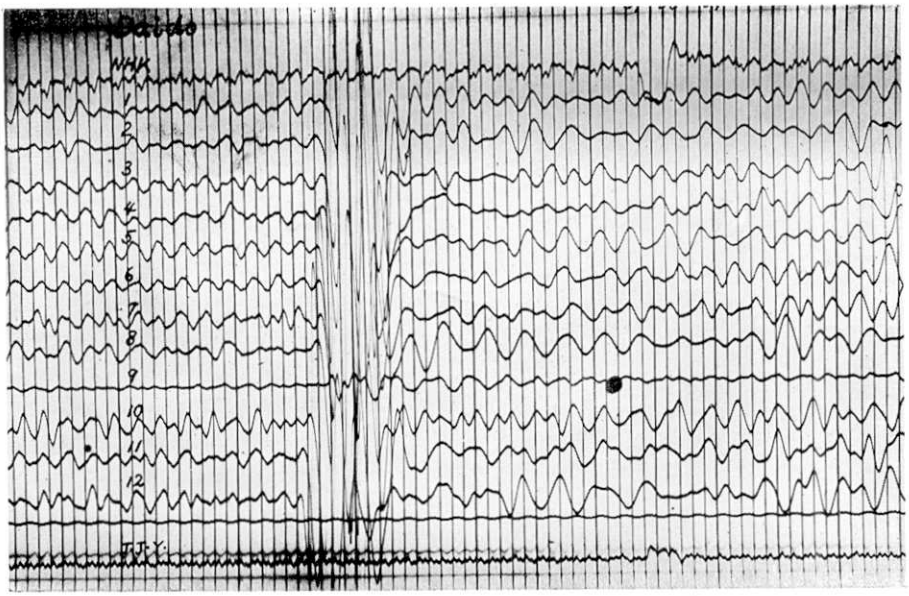

Fig. 16 (3). Seismogram at Asigase for shot C.

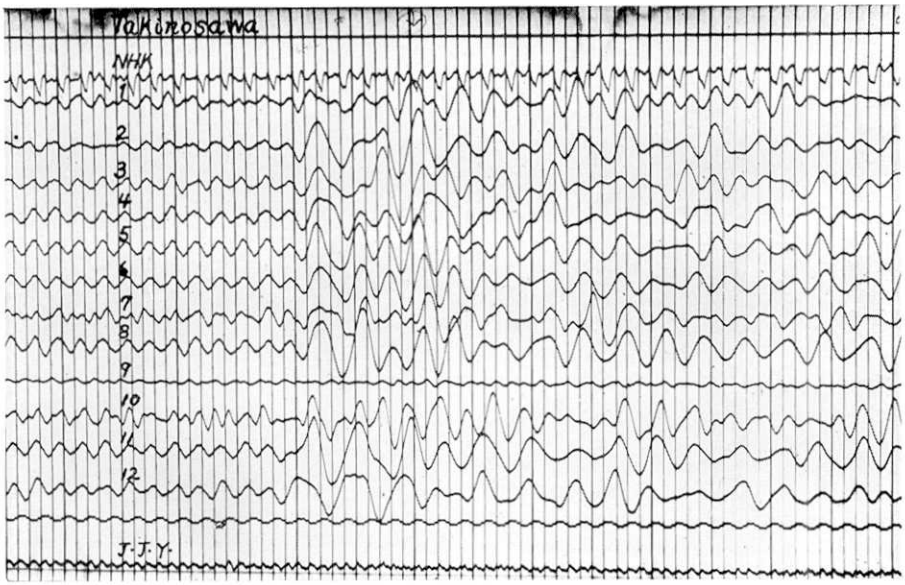

Fig. 16 (4). Seismogram at Asigase for shot D.

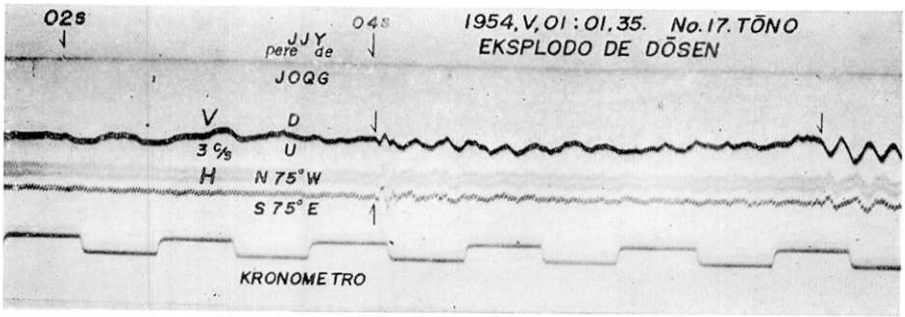

Fig. 17 (1). Seismogram at Tôno for shot A.

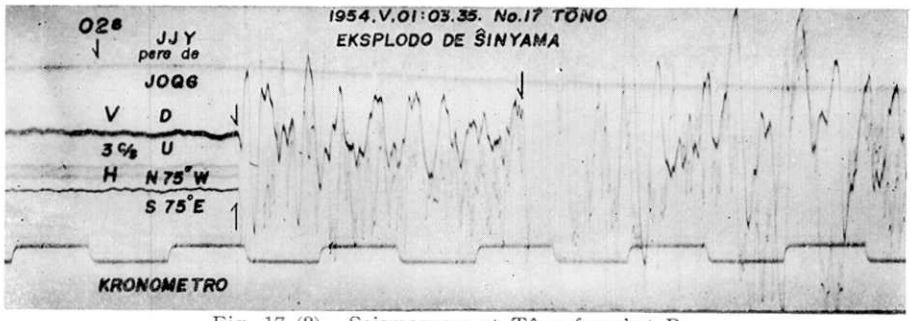

Fig. 17 (2). Seismogram at Tôno for shot B.

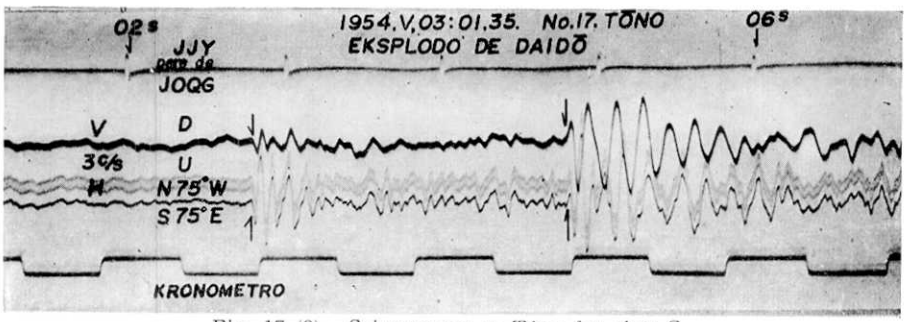

Fig. 17 (3). Seismogram at Tôno for shot C.

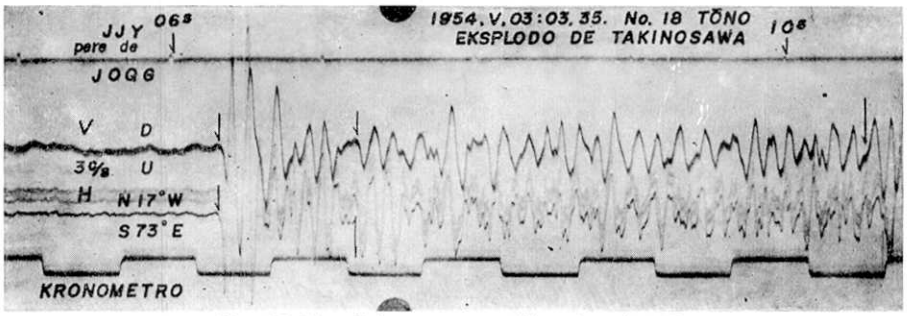

Fig. 17 (4). Seismogram at Tôno for shot D.

In Fig. 22 travel times for all shot points are plotted in such a way, that all shot points are on a common axis of abscissa, however, point B is put at the same position as point C. Travel times belonging to one and the same shot point are grouped into two branches, which correspond to the east side and west side relative to the shot point. The epicentral distance is taken as the abscissa, however, it is not the distance projected on the east-west section but the true distance.

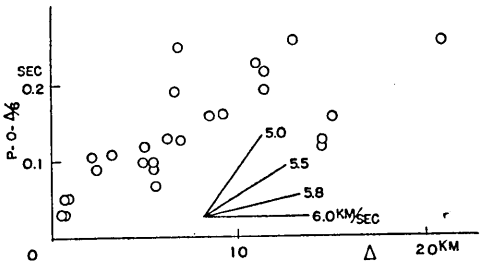

Fig. 18. Travel time for shot A.

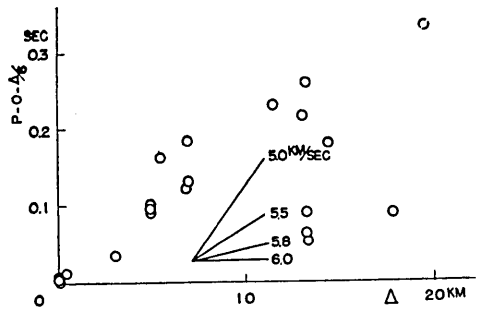

Fig. 19. Travel time for shot B.

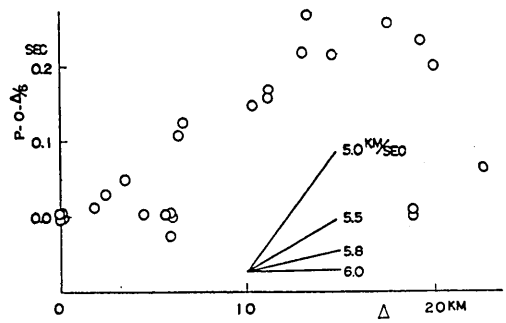

Fig. 20. Travel time for shot C.

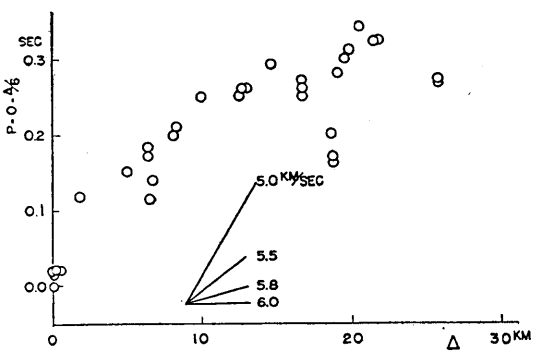

Fig. 21. Travel time for shot D.

2. Principles for deducing a structural model from the observed data.

In deducing a structural model the following guiding principles are adopted:

(a) To adopt as simple a model as possible, that means, a model which can explain well the observed data with the least number of probable assumptions.

(b) To make the difference between the observed travel time T_0 and the travel time T_c calculated from the assumed model, lie within the limit of ± 0.03 sec. For a few points under special circumstances this condition is neglected.

Table 3. Arrival time of tremors at the third Kamaisi explosion set.

SHOT TIME	A. DÔSEN 0.28 sec							B. SIN'YAMA 0.513 sec						
	L	S	A	P	Δ	$P-O-\Delta/6$	Θ	L	S	A	P	Δ	$P-O-\Delta/6$	Θ
1. SIN'YAMA								2	SM4		0.519	0	0.006	
								3	SM1	x	0.513	0	0.000	
								5	d	u	0.957	2.470	0.032	120°13′
								6	c	x	0.842	1.897	0.013	
								8	b	u	?	1.027		
								9	a	u	0.536	0.139	0.004	
								10	a	z	0.531	〃	−0.005	
2. ÔHASI	2	a	u	1.29	5.495	0.09	314° 2′	2	a					
	3	b	z	1.29	5.615	0.07		3	a					
	4	c	z	1.30	5.495	0.10	20	4	a	y	0.63	3.500	0.05	
3. ÔMATU	3	b	x	0.78	2.437	0.09	301 13	3	b	x	1.69	6.415	0.11	135 7
	4	b	y	〃	〃	〃	〃	4	b	x	〃	〃	〃	〃
	5	b	x	〃	〃	〃	〃	5	c	y	1.74	6.629	0.125	135 31
	6	c	y	0.74	2.171	0.109	310 40							128 7
4. DÔSEN	4	a	x	0.46	0.753	0.05	7 42							128 23
	5	b	x	0.41	0.592	0.03	357 40							127 32
	6	c	x	0.43∼0.44	0.760	〃	24 4							125 51
	7	d	xy	0.49	0.982	0.05	46 4							
5. MATUKURA	2		x	0.92	3.177	0.11	62 9	2		x	2.38	10.325	0.149	115 39
6. NODA	2	b	z	1.20	4.913	0.101		2	b	x	2.65	11.831	0.17	110 39
	3	a	y	1.22	4.921	0.120	68 25	3	a	x	2.64	11.822	0.16	110 33
	4	a	y	1.22	4.921	0.120		4	a	x	〃	〃	〃	〃
7. KOSANO	2	b	u	1.660	6.774	0.251	} ?	2	b	u	2.99	13.247	0.27	{105 16
	3	b	u	1.626	〃	0.219		3	b	u	2.99	13.247	0.27	} ?
	4	a	yz	1.576	6.618	0.193		4	a	u	2.91	13.097	0.22	105 6
8. NAKATUMA	2		x	1.86	8.513	0.16	66 16	2		x	3.16	14.590	0.218	101 23
								3		x	〃	〃	〃	

(to be continued)

(continued)

9. TAKINOSAWA	3 c	xy	2.693	12.895	0.26	76 44	2 c 3 c	z x	3.97 〃	19.335 〃	0.237 〃	99 5
10. KAMAISI-KO												
11. URESI	1,2	y	2.33	10.943	0.23	76 45	2 3	y y	3.70 〃	17.565 〃	0.262 〃	100 49
12. TÔNI	1 2	y y	2.38 2.40	11.414 〃	0.196 0.22	109 1	1 2	u u	4.03 〃	19.909 〃	0.202 〃	119 12
13. OKIRAI	2 3	x x	2.83 2.82	14.509 〃	0.13 0.12	163 51	2 3	y y	4.34 〃	22.590 〃	0.065 〃	151 55
14. HIKOROITI							1 b	u	3.67	18.897	0.010	Down 183 56
	2 a	y	2.96	15.108	0.16	211 6	2 a	u	〃	18.971	0.002	183 38
	3 a	y	〃	〃	〃		3 a	u	〃	〃	〃	183 56
15. DAIDÔ	3 a	x	1.45	6.252	0.13	271 12	3 a	u	1.46	5.681	0.003	178 40
	4 b	x	1.56	6.900	0.13	269 36	4 b	u	1.47	5.980	−0.020	182 4
	5 b	z	1.56	〃	〃		5 c	y	1.52	6.023	0.006	183 30
	6 b	y	1.56	〃	〃		6 d	y	1.52	6.043	0.003	〃
16. ASIGASE	3 a	u	2.002~2.004	9.303	0.171~0.173		2 a	x	1.309	4.447	0.055	
	4 b	u	2.001~2.004	9.315	0.168~0.171		3 b	x	〃	4.474	0.050	
	5 c	u	2.002~2.004	9.327	0.167~0.169		4 c	x	1.314	4.501	0.051	
	6 d	u	2.001~2.004	9.341	0.164~0.167		5 d	x	1.317	4.528	0.049	
	7 e	u	2.001~2.004	9.354	0.162~0.165		6 e	x	1.314	4.555	0.042	
	8 f	z	2.000~2.003	9.372	0.158~0.161		7 f	x	1.318	4.582	0.041	
	9 g	z	1.999~2.002	9.381	0.155~0.158		8 g	x	1.321	4.592	0.043	213 28
	10 h	z	1.998~2.002	9.356	0.159~0.163		9 h	x	〃	4.580	0.045	
	11 i	z	1.994~2.000	9.330	0.164~0.170		10 i	x	1.327	4.567	0.053	
	12 j	z	1.992~1.998	9.305	0.161~0.167		11 j	x	1.321	4.554	0.049	
	13 k	y	1.986~1.991	9.280	0.159~0.164		12 k	x	1.318	4.542	0.048	
	14 l	y	1.983~1.998	9.255	0.160~0.165		13 l	x	1.315	4.530	0.047	
17. TÔNO	2	x	4.03	20.962	0.26	289 15	2	x	2.91	13.294	0.184	273 57
	3	x	〃	〃	〃		3	x	〃	〃	〃	

(to be continued)

Table 3. (Continued)

SHOT TIME	C. DAIDÔ 0.170 sec							D. TAKINOSAWA 0.513 sec						
	L	S	A	P	Δ	$P-O-\Delta/6$	Θ	L	S	A	P	Δ	$P-O-\Delta/6$	Θ
1. SIN'YAMA	7	c	u	1.772	5.145	0.745		7	b	z	3.76~3.77	18.546	0.16~0.17	
	8	c	u	〃	〃	〃								
2. ÔHASI								2	b	y	3.57	16.729	0.27	
								3	b	y	3.56	〃	0.26	
								4	b	x	3.55	〃	0.25	
3. ÔMATU	2			not identified										
	3	b	x	1.084	4.943	0.090	76 08	3	b	y	3.25	14.698	0.29	264 30
	4	b	x	1.089	〃	0.095	〃	4	b	y	〃	〃	〃	
	5	b	x	1.094	〃	0.100	〃	5	b	y	〃	〃	〃	
	6	c	u	1.240	5.454	0.161	disturbed							
4. DÔSEN	3	a	x	1.450	6.898	0.131	85 46	3	a	x	2.89	12.730	0.26	260 56
	4	e	y	1.502	6.885	0.185	86 26	5	b	x	2.92	12.865	0.26	260 08
	5	b	x	1.425	6.800	0.122	87 32	6	c	x	2.85	12.533	0.25	260 33
5. MATUKURA								2		x	2.42	9.945	0.25	262 41
6. NODA	2		u	not clear, disturbed				2	a	y	2.07	8.154	0.20	263 14
	3	a	u	2.31	11.458	0.23	obscure	3	a	x	〃	〃	〃	〃
							82 12	4	b	x	2.08	8.162	0.21	263 23
7. KOSANO	2	b	u	2.642	13.270	0.260	?	2	b	y	1.749	6.381	0.172	267 47
								3	b	y	1.762	〃	0.185	〃
	4	a	u	2.572	13.111	0.217		4	a	y	1.760	6.545	0.116	267 40
8. NAKATUMA								1		x	1.47	4.887	0.15	278 10
								2		x	〃	〃	〃	
								3		x	〃	〃	〃	

(to be continued)

(continued)

9. TAKINOSAWA	6 c	y	3.705	19.498	0.285	83 19	1 SM	x	0.513	0	0.000		
	7 c	x	3.702	〃	0.282		5 e	x	0.618	0.504	0.021		
	8 c	x	3.705	〃	0.285		6 c	x	0.575	0.251	0.020	326 01	
							7 c	x	0.576	〃	0.021		
							8 c	x	0.575	〃	0.020		
							9 d	x	0.591	0.344	0.021		
							10 b	x	0.555	0.153	0.016		
							11 a	x	0.548	0.088	0.020		
10. KAMAISI-KO													
11. URESI	1	u	3.362	17.729	0.237	82 03	1	y	0.96	1.999	0.12	253 33	
			−3.539		∼0.414		2	y	〃	〃	〃		
12. TÔNI	Disturbed, cannot be identified						1	x	1.77	6.737	0.14	Doubt on parallax	
							2	y	〃	〃	〃		
13. OKIRAI	2	x	3.254	17.857	0.108	142 38	2	y	3.82	18.679	0.20	206 43	
		y	Time mark, not clear				3	y	〃	〃	〃		
14. HIKOROITI	1 b	y	2.429	13.171	0.064	184 52	1 b	x	5.088	25.829	0.270	232 50	
	2 a	y	〃	13.244	0.052	184 25	2 a	x	5.080	25.801	0.267	232 33	
	3 c	u	2.455	13.171	0.090		3 c	y	5.096	25.855	0.274		
15. DAIDÔ	3 a	x	0.258	0.458	0.012	82 50	3 a	x	3.96	19.033	0.28	262 53	
	4 b	x	0.223	0.301	0.003	181 56	4 b	x	4.09	19.649	0.30	262 35	
	5 c	x	0.246	0.421	0.004	229 50	5 c	z	<4.14	19.930	<0.31	261 51	
	6 d			0.442	induction by shot		6 d	z	<4.19	20.065	<0.34		
	7 SM		0.170	0	0.000								
16. ASIGASE	3 a	x	0.723	3.088	0.038		4∼10	y	4.46	21.735 ∼21.805	0.32 *P* obscure	268 28	
	4 b	x	0.717	3.080	0.034								
	5 c	x	0.719	3.072	0.037								
	6 d	x	0.719	3.064	0.038								
	7 e	x	0.712	3.056	0.033								
	8 f	x	0.713	3.048	0.035								
	9 g	x	0.715	3.043	0.038	309 23							
	10 h	x	0.711	3.026	0.035								
	11 i	x		3.009									
	12 j	x	0.704	2.992	0.035								
	13 k	x	0.699	2.995	0.030								
	14 l	x	0.693	2.958	0.030								
17. TÔNO	2	x	2.790	14.638	0.181	297 10	2	y	6.32	32.718	0.36	277 19	
	3	x	〃	〃	〃		3	y	〃	〃	〃		

L; line number reckoned from top to bottom on the original seismograms.
S; position of pick-up whose elements are given in Table 2.
A; accuracy of readings of the initial phase classified as follows:

x	y	z	u
<0.01 sec	<0.02 sec	<0.03 sec	>0.03 sec

At many places, late phases as well as the S phase were clearly observed, however, the travel time of the first P phase was exclusively used in this analysis.

3. The first approximation to the model in the east-west vertical section.

As apparent from Fig. 1, it may be safely assumed that shot points A, B, C, D, and observation points 1～11, 15, 16 and 17 approximately lie in a common east-west profile. Therefore, from travel times at these places, the first approximation of the model in this section is deduced.

First, if we compare the travel time at point 9 from shot A with that at point 4 from shot D (Table 3), the difference is very small i.e. 0.01 sec. This fact fulfils the condition that the ray path is common between both shots.

If travel times at points 4～11 from both shots A and D are plotted in a figure (Fig. 23), points belonging to shot A are arranged on a line clearly different from that through points belonging to shot D. The

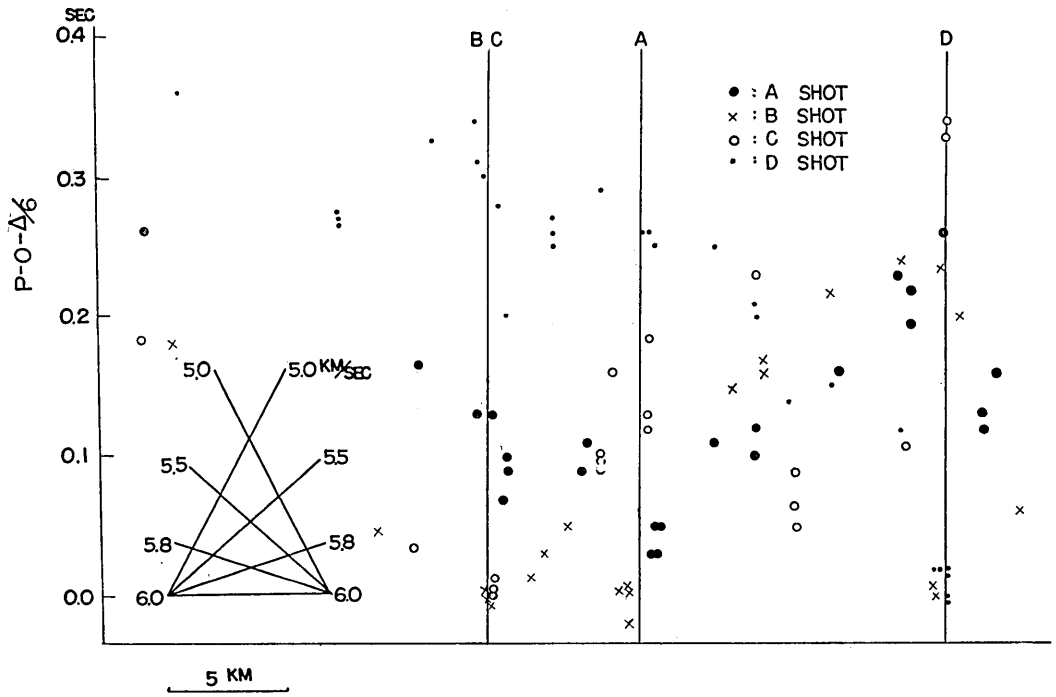

Fig. 22. Travel time for shot A, B, C, and D transferred to the section CAD.

apparent velocities are deduced respectively as 5.45 km/sec and 5.54 km/sec. Therefore, their mean value 5.50 km/sec is taken as the true velocity in the second layer.

In Fig. 23 another branch of travel time curves is observed at points near the shots. Its approximate velocity is given as 4.5 km/sec, and this value is adopted as the velocity in the first layer. The point of intersection is at a distance of 0.78 km for shot A and 2 km for shot D. Hence the depth of the first layer is 122 m at A and 314 m at D. Consequently the dip of the boundary between layer 1 and layer 2 is $\theta_{1,2}=50.3'$ to the east.

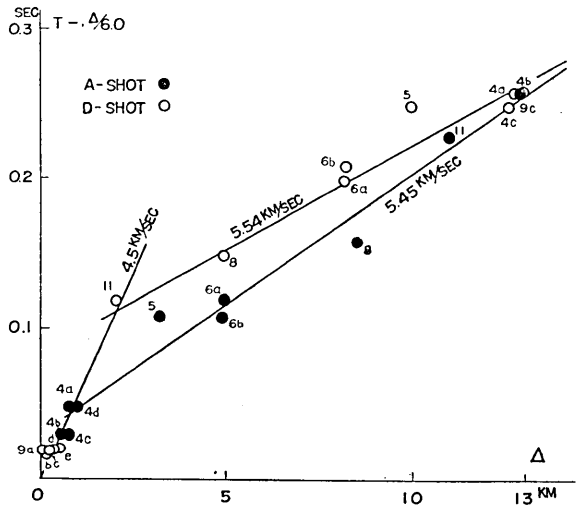

Fig. 23. Travel time for shots A and D.

Next, from the eastward branch of the travel times for shot B (Fig. 19) the apparent velocity V_s is found slightly larger than $V_2=5.5$ km/sec, with no intercept time. Therefore, it is inferred that there is a third layer with true velocity larger than V_s and the boundary between layer 2 and layer 3 dips toward the east and layer 3 is almost exposed at point B. Exact value of the true velocity of layer 3 is yet uncertain. In Fig. 21 point 16 and point 17 for shot D lie probably on the farthest branch, which shows the apparent velocity 5.86 km/sec and the break point at 14 km from the shot point. Adopting a triple layered model and using V_1, V_2, $\theta_{1,2}$ and apparent velocity 5.86 km/sec, a set of dip angles of the boundary between the second and the third layer, $\theta_{2,3}$ can be calculated, taking V_3, the velocity in the third layer as the parameter. (Table 4)

Table 4.

V_3	$\theta_{2,3}$
5.78 km/sec	1° 3′ 20″
5.80	30 20
5.82	−6 40

As obtained before, the boundary must dip eastward. Therefore, V_3 must be less than 5.81 km/sec. Thus we infer that $V_2=5.8$ km/sec

in the former paper[2] corresponds to V_3 in this case, and put $V_3=5.8$ km/sec. Assuming this value and $\theta_{2.3}=30'$, and taking travel times at point 16 and 17 into consideration, the following relation between the thickness of the second layer h km at D and the distance Δ_c km of the break point of the travel time curve is deduced. Namely,

$$h=0.0808\Delta_c-0.0659\,.$$

For $\Delta_c=14$ km, h turns out 1.05 km.

From travel times at point 14 and point 15 for shot B, i.e. in the nearly N–S profile, an apparent velocity 6.0 km/sec is got. Comparing the result in the former paper, 6.2 km/sec is adopted as V_4 in this case. In this profile, assuming a horizontal double layered model with layers V_3 and V_4, the sum of the thickness of the V_3 layer at shot B and at point 14 is calculated as 1.5 km. Therefore, the depth of the upper boundary of the fourth layer seems comparatively shallow in the B–C

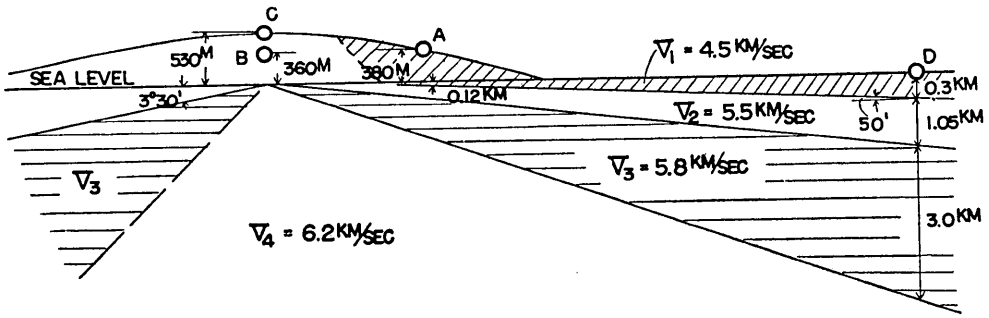

Fig. 24. First approximation to the crustal model in section CAD.

section. From the southward profile for the D-shot, the depth to the fourth layer at point D seems somewhat deep, however, its exact value cannot be given. Taking the westward travel times for shot D into account, we tentatively put the depth equal to 4.5 km. The travel times at point 17 for shot B and C seem to belong to the path through layer 3.

If we assume that the top edge of the third layer be at sea level, the dip of the upper surface toward the west is calculated $\theta'_{2.3}=4°20'$ from shot B and $\theta'_{2.3}=2°50'$ from shot C. The mean value 3°30′ is taken as the first approximation.

From above considerations, a section as shown in Fig. 24 is taken as the first approximation.

2) *loc. cit.*, 1).

4. Determination of the east-west profile.

For further approximation, heights of the observation points and shot points, which were neglected in the first approximation, are taken into account. Starting from the approximate structure in Fig. 24, by the trial and error method we get the final structure as shown in Fig. 25, which is so determined that the O–C residues as a whole remain within the limit 0.03 sec. The residues thus calculated are shown in Table 5.

No sufficient data are at hand for the exact determination of the position of the boundary between the third and the fourth layer. How-

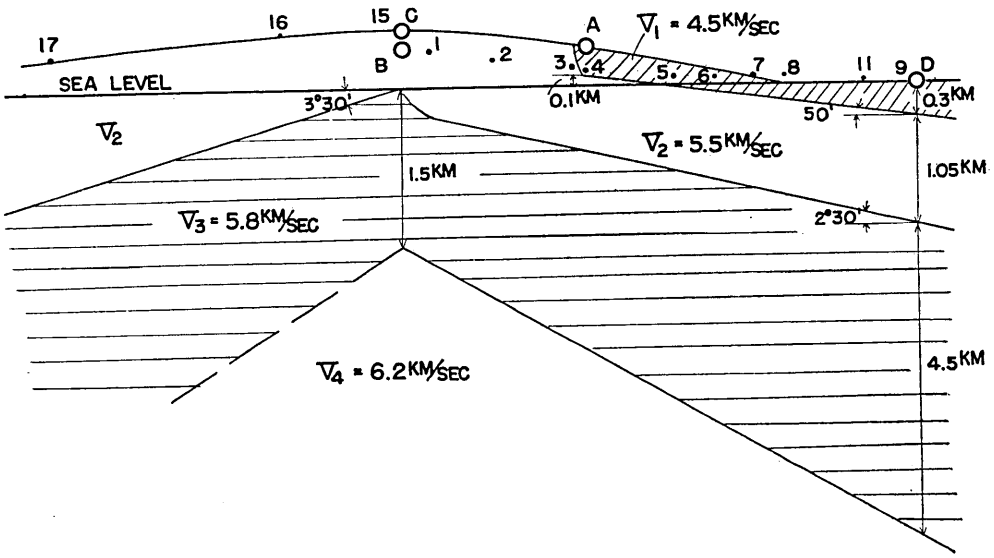

Fig. 25. Final result of the crustal model in section CAD.

ever, it is qualitatively doubtless that it dips down away from the B shot. The third and fourth layers in this report respectively correspond to the P_2 and P_3 layer in the former paper.[3)]

The presumption stated in the former paper, that the P_2, P_3 boundary should rise eastward and almost appear on the surface near the Kamaisi mine, is confirmed in this study.

5. Underground structure in the southern part.

We have 3 observation points, 12, 13, and 14 in the south. The unique determination of the underground structure from these scanty

3) *loc. cit.*, 1).

Table 5. T_0–T_c (unit in sec)

Station & P. U. Position \ Shot		A		B		C		D	
1	c			−0.024	II				
	d			−0.007	〃				
2	a	−0.035	I, II	−0.008	〃				
	b	−0.045	〃					0.04	I, II, III
3	b	0.006	〃	0.00	I, II	0.01	II	0.04	〃
	c	0.015	〃	0.013	〃				
4	a	0.007	I			−0.016	I, II	0.02	I, II, III
	b	0.000	〃			0.02	〃	0.03	〃
	c	−0.007	〃					0.01	〃
	d	−0.007	〃						
5		−0.025	I, II	−0.04	I, II			0.03	I, II
6	a	−0.035	〃	0.02	I, II, III	0.03	I, II, III	0.00	〃
	b	−0.055 (z)	〃	0.03	〃			0.01	〃
7	a	0.015	〃	0.04 (u)	〃	0.012	〃	−0.02	〃
	b	0.035	〃	0.08 (u)	〃	0.048	〃	0.01	〃
8		−0.015	〃	−0.01	〃			−0.009	〃
9	a							0.015	I
	b							0.008	〃
	c	−0.005	I, II, III	−0.01	I, II, III	−0.02	I, II, III	0.006	〃
	d							0.002	〃
	e							−0.007	〃
11		−0.026	I, II, III	0.025	I, II, III	−0.01	I, II, III	0.005	〃
12		**0.04**	〃	**0.06**	II, III			**0.01**	I, II, III
13		**−0.018**	〃	**−0.05**	II, III, IV	**−0.008**	II, III or II, III, IV	**0.00**	〃
14	a	**0.05**	I, II, III, IV	**0.015**	〃			**0.11**	I, II, III, IV
	b			**0.015**	〃	**−0.01**	III	**0.12**	〃
	c					**−0.03**	〃	**0.12**	〃
15	a	−0.015	I, II	**−0.05**	II, III	0.005	II	**0.03**	I, II, III
	b	−0.020	〃	**−0.08**	〃	0.00	〃	0.05	〃
	c			**−0.08**	〃	0.00	〃		
	d			**−0.08**	〃				
16	a			−0.008	II	−0.01	II	−0.06	I, II, III
	c			−0.018	〃	−0.008	〃		
	e	0.00	I. II	−0.03	〃	−0.015	〃		
	1					−0.018	〃	−0.04	I, II, III
17		−0.003	I, II, III	0.015	II, III	0.00	II, III	0.17	I, II, III, IV

I, II, ...denote layers through which the wave, that reached the observation point at first, passed. Values of O-C in Gothic type are obtained by the method of § 5.

data is almost impossible. Thus we must resort to search for such a model, which is compatible with the result in the east-west section and makes the O–C residues at these points as small as possible.

To begin with, a profile B-C-14-15 is tried, taking travel times at point 14 and 15 for shot B and at point 14 for shot C into consideration. Referring to the former results, we assume point 14 is on the boundary between the third and fourth layer, the boundary between the second and third layer under point B and C is at sea level, and the thickness of the V_3 layer is 1.5 km under point B. (Fig. 25)

From these assumptions, a model shown in Fig. 26 is obtained.

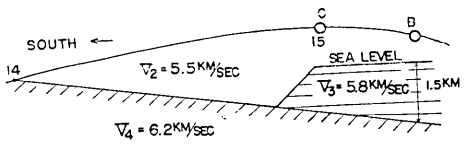

Fig. 26.

Layer V_3 is cut off slightly in the south under point C, otherwise the travel time at point 14 for shot C comes out too early. O–C values calculated from the Fig. 26 model are shown in table 5.

Next, a profile D–12, 13 and 14 is tried, taking travel times at these points into account. Though point 14 deviates from the line D–12–13, for the sake of approximation, the point is brought on to the line, while maintaining its distance from shot D.

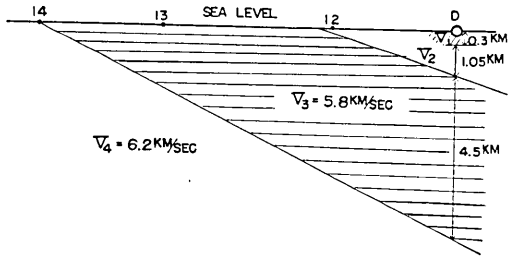

Fig. 27.

Again referring to Fig. 25 and assuming point 14 on the V_3–V_4 boundary, we get a model shown in Fig. 27. The V_2–V_3 boundary is determined in such a way that the residue O–C at point 12 be nearly zero. The wave path in this case should pass through the V_3 layer.

Referring to Fig. 25, 26, and 27, the depth of each boundary under each shot point and observation point is given. Thus, travel times for all combinations of shot points and observation points can be calculated. In this procedure, slight interpolations to the position of the boundary are taken for granted. For example, in the profile A–14, as the depth of each boundary is given at A and 14, connecting each corresponding boundary, we take the connecting line as the corresponding boundary under A–14 section.

As for the V_2–V_3 boundary in section A–14, the boundary in Fig.

27 is prolonged to the vertical line at point 14, and its intersection point is connected to the corresponding point under A. Thus we can calculate the travel time at point 14 from shot A.

O-C residues thus obtained are tabulated in Table 5.

6. Concluding remarks.

There may remain some freedom as to the true velocity in the V_1 layer, its thickness, and the position of the V_3–V_4 boundary. That is to say, they may be subject to some change without changing O-C residues much. Of course, it is possible to add some mutually independent assumptions to the underground structure, in order to ameliorate each O-C residue, for example, to insert a certain very local singularity in the path of waves. This means to add one assumption to one datum. Such a way of procedure is excluded from our guiding principle stated in 2.

Geologically speaking, the dotted line in Fig. 1 is a boundary between granite and palaeozoic strata, which is almost coincident with the boundary between the V_2 and V_3 layers.

In this report the observed data were compiled mainly by S. Asano and the part concerning the crustal structure was compiled mainly by T. Usami.

We are much obliged to the prefectural authorities of Morioka, Huzi-Seitetu Company, Morioka Department of Japan Government Railway, the Technical Department of Tôkyô Central Station and Morioka Branch Station of NHK., provincial authorities and police stations at each temporary observation station, for much indispensable help and facilities given by them.

6. 釜石鉱山附近4回の爆破地震動の観測について

爆破地震動研究グループ

すでに行われた石淵 3 回および釜石鉱山 2 回の大爆破の観測結果を綜合して，東北地方の地下構造が推算された．そのとき得られた地層のうち，P 波速度 5.8 km/sec および 6.1 km/sec の 2 層の境の面のありさまは，特に興味あるものであるが，その東辺の構造が充分よくわからなかつたので，おもに，それをきめるために，釜石鉱山および釜石港附近の 4 点の爆破のくわしい観測を行つたものである．

爆破点については表 1，観測点については表 2 に示され，その位置のあらましは，第 1 図にも示してある．走時その他は表 3 にくわしく示され，又走時図は図 18～22 に示すとおりである．

地下構造の東西断面については第 25 図，南北断面（ふたつの断面）については，第 26 図および第 27 図のようなものが推定される．